Advances in Science and Technology Research Journal

Advances in Science and Technology Research Journal, 2026, 20(7), 521–531
https://doi.org/10.12913/22998624/220471
ISSN 2299-8624, License CC-BY 4.0

Received: 2026.02.14
Accepted: 2026.05.15
Published: 2026.06.01

Research on die-casting defect control by spot cooling water and heat treatment strengthening for ADC12 engine cylinder block

Zhiwei Tang[1], Yongzheng Zhao[1], Xinyu Huang[1], Chao Lu[2], Li Heng[1,3*], Yu Cheng Wu[1]

[1] School of Materials Science and Engineering, Hefei University of Technology, Hefei 230009, China
[2] Hefei Yaming Auto Parts Co., Ltd., Hefei 230009, China
[3] Anhui Province Key Lab of Aerospace Structural Parts Forming Technology and Equipment, Hefei University of Technology, Hefei 230009, China
* Corresponding author's e-mail: liheng0205@hfut.edu.cn

ABSTRACT

To improve the internal quality and mechanical properties of ADC12 aluminum alloy engine blocks, this study optimizes the die-casting process and T6 heat treatment via numerical simulation and experimental analysis. A spot cooling water system was integrated into the thick-walled mold regions to control solidification at a 660 °C pouring temperature. Results indicate that optimized spot cooling significantly reduced air entrainment and shrinkage porosity to 3,237.06 mm³ and 503.12 mm³, respectively, satisfying heat treatment requirements. Microstructural analysis reveals that solution treatment (520 °C, 3 h) facilitates the complete dissolution of the Al_2Cu phase into the α-Al matrix. After aging at 180 °C for 8 h, the tensile strength and yield strength reached 312.8 MPa and 239.6 MPa – increases of 40.2% and 58.5% over the as-cast state. This optimal 520 °C × 3 h + 180 °C × 8 h process ensures high mechanical performance and dimensional stability while significantly shortening the production cycle compared to longer aging durations.

Keywords: ADC12 aluminum alloy, vacuum die casting, casting defects, T6 heat treatment.

INTRODUCTION

ADC12 aluminum alloy is a prominent Al-Si-Cu casting alloy. It is widely used as a core structural material in automotive lightweighting and electronic packaging due to its superior castability, high specific strength, and cost-effectiveness. High-pressure die casting (HPDC), characterized by its high production efficiency and capability for forming complex geometries, is widely utilized in the manufacturing of intricate housing parts, such as engine blocks [1]. High-pressure filling often triggers violent air entrainment. Combined with insufficient feeding in regions distant from the gate, this process frequently introduces internal defects like gas pores and shrinkage porosity [2]. These void defects not only directly split the matrix and create stress concentrations, thereby reducing the as-cast strength, but also significantly compromise the mechanical integrity of the components. Furthermore, such defects can lead to severe surface blistering during subsequent heat treatment processes [3,4]. These defects represent a major technical bottleneck. They prevent T6 heat treatment (solution treatment, quenching, and aging) from further enhancing the mechanical properties of die-cast ADC12 alloys. Therefore, preliminary optimization of the die-casting process is essential to reduce internal casting defects, providing a dense microstructural foundation for subsequent heat treatment. T6 heat treatment is the core method for synergistically enhancing the comprehensive mechanical properties and dimensional stability of Al-Si alloys. During the solution treatment stage, the heating temperature must be strictly controlled below the low-melting-point

eutectic temperature to prevent localized overburning at grain boundaries. Under this premise, appropriately increasing the solution temperature can significantly accelerate the dissolution rate of strengthening phases and maximize the solid solubility of alloying elements such as Cu and Mg within the α-Al matrix. Subsequently, a supersaturated solid solution is obtained through rapid quenching, which induces the uniform and dispersed precipitation of nanoscale metastable phases (e.g., θ'-Al_2Cu) during the following artificial aging stage. Consequently, a significant leap in the macroscopic mechanical properties of the alloy is achieved through the precipitation strengthening mechanism[5].

Extensive studies have been conducted by scholars to enhance the performance of die-cast components. Regarding the optimization of the die-casting process, Jiao X et al. [6] and Xiao R et al. [7] investigated the influence mechanisms of injection speed on the microstructural framework during high-pressure die casting (HPDC). Cao H et al. [8] studied the effect of porosity on the mechanical properties of vacuum die-cast parts. Zhang Mingyu et al. [9] addressed issues such as shrinkage porosity, gas pores, and insufficient strength in ADC12 castings by optimizing pouring temperature, specific pressure, and filling speed. Concerning heat treatment strengthening mechanisms, Yunfei et al. [10] and Xu Weiming et al. [11] explored the effects of various solution and aging parameters on microstructures, noting that appropriate heat treatment can induce the dispersed precipitation of strengthening phases like Al_2Cu within the supersaturated solid solution, thereby significantly enhancing both the strength and corrosion resistance of the alloy. By utilizing Al-Si alloys containing Cu and Mg and applying suitable heat treatments, the precipitation hardening of Al_2Cu and Mg_2Si intermediate phases [12,13] has yielded high-strength alloys suitable for high-quality die casting.

However, most existing studies treat the die-casting process and heat treatment as isolated stages, or focus solely on heat treatment mechanisms using defect-free idealized specimens or high-vacuum die-cast parts. There is a lack of systematic, synergistic research targeting real high-pressure die-cast engine blocks with complex internal cavities that bridges "die-casting defect control" and "heat treatment strengthening."

Given that optimizing a single conventional die-casting process is no longer sufficient to break the mechanical performance bottleneck of current high-performance engine blocks, this study focuses on ADC12 aluminum alloy die-cast engine blocks and proposes a synergistic regulation strategy of "die-casting defect control and T6 heat treatment strengthening". First, the pouring temperature and cooling system were optimized based on filling and solidification characteristics to significantly improve internal microstructural uniformity and reduce defect volume, thereby providing a prerequisite guarantee for subsequent heat treatment. On this basis, the T6 heat treatment process was introduced to precisely regulate the microstructural evolution and precipitated phases of the alloy. This research aims to overcome the limitations of performing standard T6 heat treatment on high-pressure die castings, fundamentally resolve the issue of insufficient strength in engine blocks, and achieve a dual leap in both microstructural refinement and comprehensive mechanical performance.

MANUFACTURING PROCESS OF ENGINE BLOCKS

Structural characteristics and technical challenges of the casting

The engine block possesses overall dimensions of 380 × 340 × 300 mm, with a casting volume of 6.5 × 106 mm^3 and a blank mass of approximately 18 kg. The average wall thickness of the casting is 6.92 mm, with a maximum thickness of approximately 33.02 mm and a minimum of 4.32 mm, as illustrated in Figure 1. It is evident that the casting exhibits a highly non-uniform wall thickness distribution with significant thickness variations, a complex external geometry, and a lack of symmetrical features. The internal through-holes vary in shape and size, being irregularly distributed; meanwhile, the outer surface is rich in curved structures, further increasing the irregularity of the profile. Furthermore, the casting features numerous internal cavities with intricate spatial layouts and complex interconnections, categorizing it as a typical complex thin-walled component.

As the core load-bearing component of the powertrain, the engine block serves under severe working conditions characterized by complex thermo-mechanical alternating loads. This imposes extremely high requirements on its comprehensive

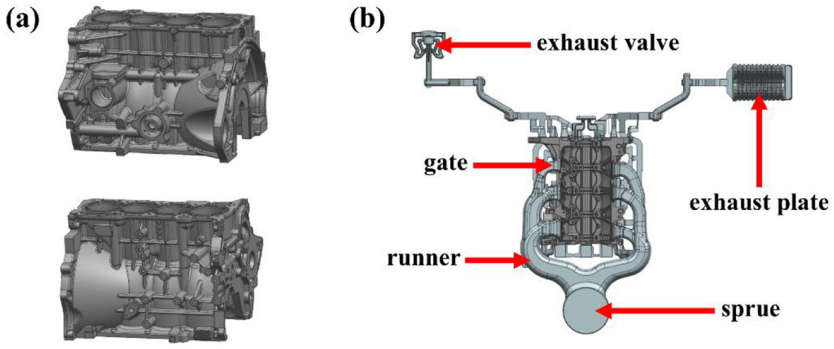

Figure 1. Casting model and gating/riser system: (a) casting model; (b) gating and overflow system

mechanical properties, including tensile strength, yield strength, fatigue life, and dimensional stability. However, limited by the complex structural features of the block and the inherent nature of high-pressure filling and rapid solidification, defects such as gas pores and shrinkage porosity are easily retained within the castings. Furthermore, the resulting non-uniform microstructure, suboptimal alloy phase distribution, and grain morphology mean that optimizing the die-casting process alone can no longer break through the existing performance bottleneck. Therefore, while ensuring the dimensional integrity of the block, it is essential to incorporate heat treatment to regulate the microstructure and enhance the performance of the as-cast alloy. The synergistic effect of these two approaches allows for a systematic improvement in the comprehensive mechanical properties of the engine block, thereby satisfying the stringent service requirements of new-generation high-power-density engines for high reliability, long service life, and lightweighting.

Materials and experimental methods

The ADC12 aluminum alloy ingots were heated to 750 °C in a melting furnace until fully melted. The melt was then refined with high-purity argon (Ar) at 0.5 MPa for 7 min before being transferred to a holding furnace. Subsequently, the melt was injected into the shot sleeve of a LK DCC2500T horizontal cold-chamber die-casting machine, and vacuum die casting was performed according to the pre-set process parameters to form the castings.

The material used in this study is grade ADC12 aluminum alloy. Its chemical composition, determined via spark atomic emission spectrometry (Spark-OES) using a MAXx07-F equipped with high-resolution CCD detectors, is presented in Table 1.

The liquidus temperature of ADC12 with this composition is approximately 580 °C. A control group was established with a pouring temperature of 660 °C, an injection speed of 4.5 m/s, and a mold temperature of 200 °C to analyze the filling and solidification patterns, as well as defect formation under different pouring temperatures.

Since the mechanical properties of the as-cast alloy cannot meet the design requirements, the die-castings were subjected to solution treatment at 520 °C for durations of 0.5 h, 1 h, 2 h, 3 h, and 4 h, followed by immediate water quenching at 25 °C. Subsequently, artificial aging was performed at 180 °C for 2 h, 4 h, 6 h, 8 h, 10 h, and 12 h, followed by air cooling.

Metallographic and mechanical property specimens were extracted from designated sections of the die-cast components. After standard mechanical grinding and polishing, the specimens were etched with Keller's reagent for 10–15 s, followed by ultrasonic cleaning in anhydrous ethanol and cold-air drying. The microstructure of the specimens under various experimental conditions was observed using an Axiocam 208 and Axiolab 5 color optical microscope (OM). Surface morphology of the etched specimens was examined using an SU8020 cold-field emission scanning electron microscope (FE-SEM) at an accelerating voltage of 5 kV in secondary electron (SE) mode, while the elemental distribution at the interface was subsequently analyzed via the integrated energy-dispersive X-ray spectroscopy (EDS) at an accelerating voltage of 15 kV. Hardness measurements were conducted on a 10VH-5 Vickers hardness tester with a load of 98 N and a dwell time of 10 s. Room-temperature tensile tests were performed using a SHIMADZU AGS-X universal testing machine at a strain rate of 1 mm/min. To ensure data reliability, three parallel specimens were tested for each process condition. Calculation methods for

Table 1. Chemical composition of ADC12 aluminum alloy (wt.%)

Si	Cu	Fe	Mg	Zn	Mn	Ni	Al
10.21	2.13	0.68	0.072	0.57	0.14	0.037	Bal.

mechanical properties: Tensile strength is defined as the maximum load divided by the original cross-sectional area. Yield strength is determined from the load-displacement curve according to standard methods. Elongation is calculated as: (gauge length after fracture – original gauge length) / original gauge length × 100%. The sampling locations are illustrated in Figure 2, where Figure 2(d) shows the dimensions of the standard tensile specimen.

DEFECT ANALYSIS AND PROCESS OPTIMIZATION OF THE ENGINE BLOCK

During the high-pressure die casting (HPDC) of engine blocks, shrinkage cavity and porosity defects are highly susceptible to forming within the casting due to localized thick sections and specific solidification characteristics. Consequently, directional sectioning was performed at the defect-prone locations. High-resolution X-ray inspection was then conducted using a YXLON FF35 CT system at a tube voltage of 220 kV, with the results illustrated in Figure 3. These void defects not only severely compromise the mechanical properties of the casting but also destroy the matrix density, rendering it incapable of withstanding the requirements of subsequent high-temperature heat treatment. To address these casting defects, this study significantly reduces the volume of internal shrinkage porosity and cavities by optimizing the pouring temperature and the localized mold cooling system. On the premise of ensuring high density, the T6 heat treatment process is incorporated to further achieve microstructural homogenization and a leap in comprehensive mechanical performance. Ultimately, this synergistic approach meets the high-reliability service standards of this engine model under rigorous operating conditions.

In this study, Flow-3D software was employed to conduct numerical simulations of the mold-filling process and solidification behavior of the engine block. The investigation primarily focused on predicting the entrained air volume during the filling stage and the evolution of shrinkage cavity and porosity distributions during solidification, providing a theoretical basis for optimizing the casting process.

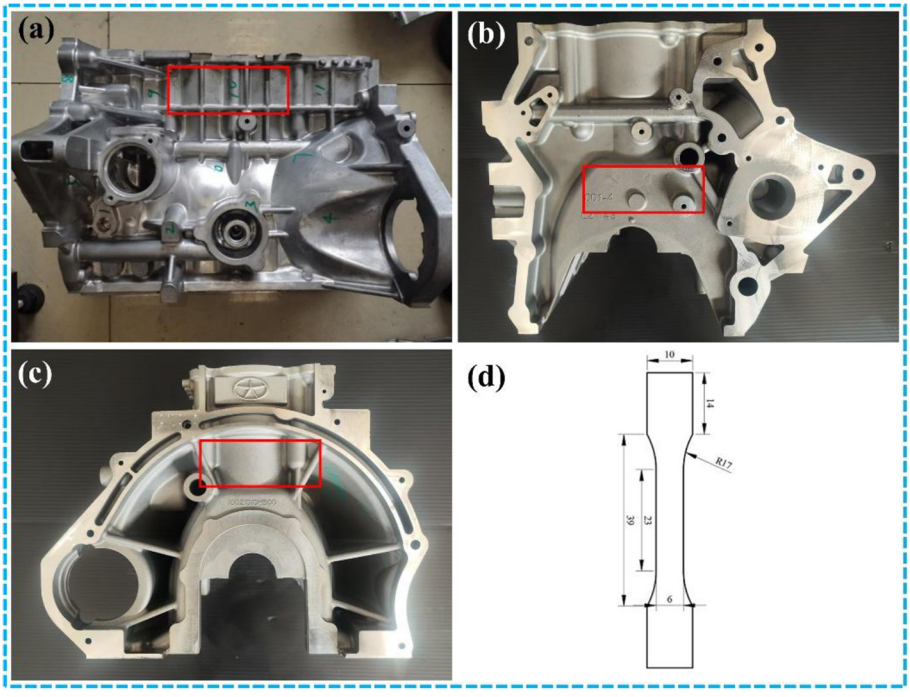

Figure 2. Schematic of sampling locations: (a) front view; (b) (c) side views; (d) dimensions of tensile specimen

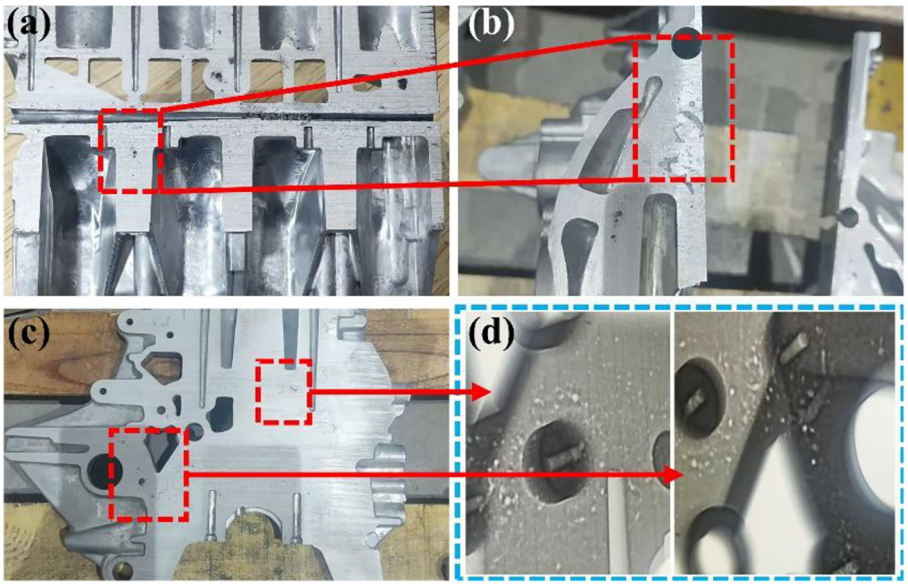

Figure 3. Internal defects of the engine block before optimization: (a, b, c) sectional view; (d) X-ray radiographic image

During the filling stage of die casting, gas trapped within the mold cavity is primarily pushed by the molten metal flow and concentrates at the cavity ends, slag bags, and overflow regions. Simulation results indicate that at a pouring temperature of 660 °C, the volume of gas entrainment within the engine block is restricted to 3,237.06 mm³. At this temperature, the melt exhibits excellent fluidity, ensuring a stable filling front and effectively suppressing the occurrence of severe splashing and turbulence. Meanwhile, the optimal melt viscosity facilitates the smooth expulsion of entrapped gases into the venting system, thereby significantly reducing the degree of gas entrainment within the effective casting area.

The solidification stage is a critical period for the formation of internal shrinkage defects. Solidification first occurs in the overflow and venting regions, followed by the casting surface and thin-walled sections; subsequently, regions near the gate begin to solidify, with the gating system being the last to solidify. Within the casting near the cylinder areas, unsolidified molten metal forms isolated liquid pools. These regions, characterized by complex geometries and greater wall thicknesses, exhibit slower cooling rates and often become the last zones to solidify. When these isolated liquid pools cannot be effectively replenished through feeding, they evolve into micro- or macro-shrinkage porosity and cavity defects.

To address the formation of shrinkage porosity and cavities in thick-walled sections and isolated liquid pools during solidification, the mold locations corresponding to the thick-walled regions and defect-prone areas of the engine block are highlighted within the red boxes in Figure 4 (a). According to the schematic of spot cooling positions in Figure 4 (b), spot cooling devices were installed at the corresponding locations within the mold. This setup significantly accelerates the cooling rate in these regions, narrows the range of the last-to-solidify isolated liquid pools, and reduces the volume of shrinkage defects caused by insufficient feeding. Consequently, the casting density and internal quality are effectively enhanced.

Combined with the cross-sectional temperature field simulation results in Figure 5(e), it is evident that the shrinkage porosity and cavity defects primarily originate at the thick-walled sections (such as the cylinder bore gaps) and structural junctions. These areas form typical "hot spots" due to localized thermal accumulation and poor heat dissipation, leading to a significant delay in solidification and the subsequent formation of shrinkage voids. Theoretically, although a higher pouring temperature (660 °C) can markedly enhance the filling capacity of the melt, the increase in the total system enthalpy further prolongs the local solidification time of these thick sections, exacerbating the volumetric shrinkage tendency of isolated liquid pools. However, by precisely incorporating spot cooling devices at the corresponding hot spots in the mold, the localized cooling rate is forcibly enhanced, effectively

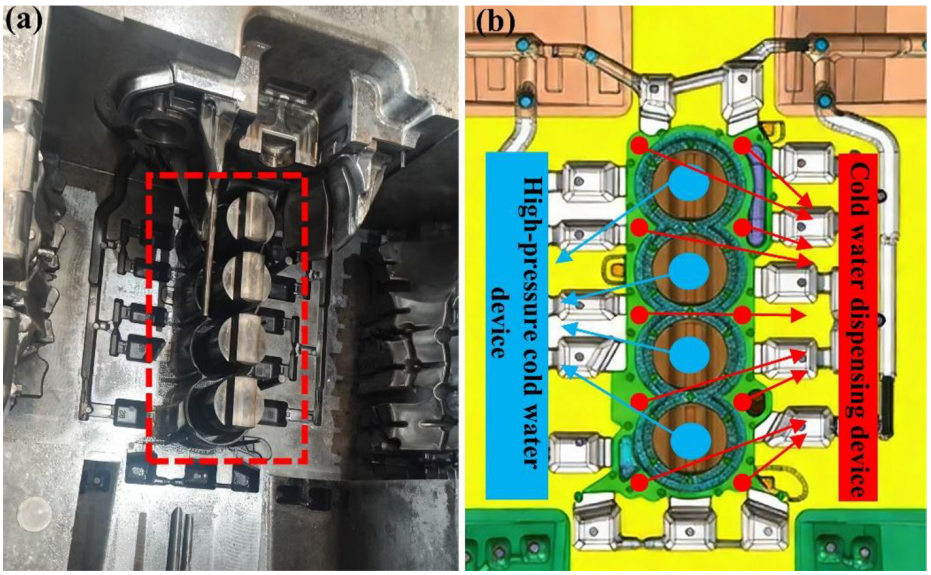

Figure 4. (a) Mold locations corresponding to thick-walled regions; (b) schematic of spot cooling water channel distribution

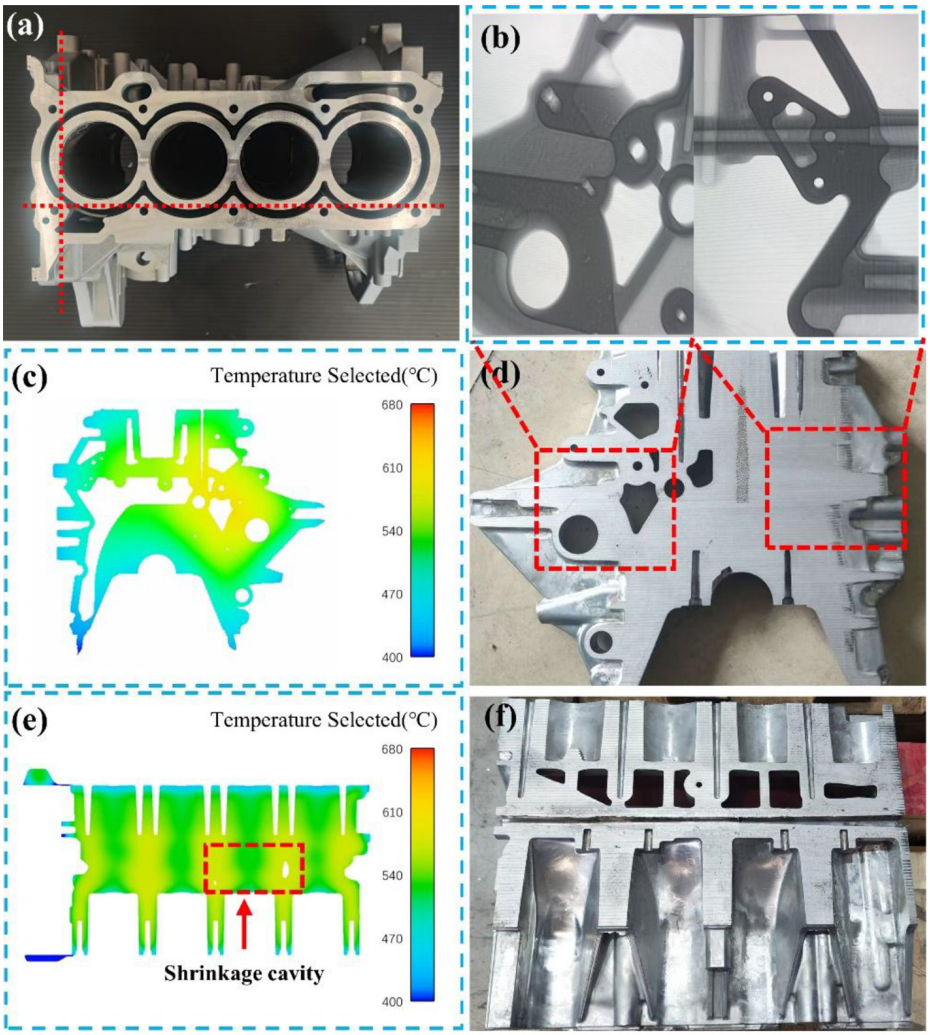

Figure 5. Cross-sectional temperature field, sectional view, and X-ray radiographic image of the casting after optimization (660 °C): (a) cross-section positions; (b) X-ray radiographic image; (c, e) cross-sectional temperature field distribution; (d, f) sectional views of the engine block

disrupting the original state of thermal accumulation. Calculation results confirm that under this optimized process (660 °C pouring + spot cooling synergy), the total volume of shrinkage defects within the block is drastically compressed to 503.12 mm³. More critically, the optimized residual pores exhibit a fine and dispersed distribution, eliminating large-scale concentrated shrinkage cavities. Their size and distribution are controlled within safe thresholds, thereby minimizing the adverse impact of micro-defects on the macro-mechanical properties of the engine block.

Although the comprehensive mechanical properties of the as-cast block still fall short of high-performance service standards at this stage, the substantial reduction in gas entrainment and shrinkage volume significantly improves the matrix density. This high-density characteristic fundamentally circumvents scrap risks, such as surface blistering and dimensional distortion, which are easily induced during the subsequent high-temperature solution treatment stage, thereby fully satisfying the prerequisites for T6 heat treatment. Based on this, subsequent research will introduce the T6 process to further achieve a leap in mechanical properties and structural strength through deep microstructural regulation and precipitation strengthening mechanisms, ultimately meeting the stringent service requirements of high-performance engines.

SOLUTION AND AGING TREATMENT

Effect of solution time on microstructure

Based on the solidus temperature characteristics of the ADC12 alloy (approximately 500–520 °C), a solution temperature of 520 °C was selected in this study to accelerate the dissolution of the Al_2Cu strengthening phase and optimize the solid solubility. This temperature window not only enhances the solution efficiency but also promotes the rapid spheroidization of eutectic silicon. By reducing the aspect ratio of silicon particles, stress concentration is effectively mitigated, thereby improving the overall plasticity and toughness of the material [14,15].

Figure 6 presents the scanning electron microscopy (SEM) images of the alloy after solution treatment for various durations. The bright regions represent the Al_2Cu phase, while the darker regions correspond to the Fe-rich phases. Compared to the as-cast alloy, the Al_2Cu phase significantly diminishes or nearly disappears after solution treatment, whereas the Fe-rich phases remain at the grain boundaries. These observations indicate that the Al_2Cu phase gradually dissolves into the α-Al matrix during solution treatment, while the Fe-rich phases exhibit negligible dissolution. To investigate the elemental distribution uniformity within the matrix, energy-dispersive X-ray spectroscopy (EDS) mapping was performed on random areas of the alloy. As shown in Figure 7, the Cu elements are uniformly distributed throughout the alloy after solution treatment. In contrast, the Fe elements are primarily concentrated at the grain boundaries, further confirming that the Fe-rich phases underwent almost no dissolution under the current solution treatment conditions.

Following solution treatment at 520 °C for 0.5 h, 1 h, 2 h, 3 h, and 4 h, the tips of the originally coarse, needle-like eutectic Si undergo fragmentation and necking, exhibiting an initial "disintegration and fracturing" phenomenon. With the further extension of the holding time, the Si particles gradually evolve from a "fractured state" to a "spheroidized state." Further observation reveals that the spheroidization of the eutectic Si phase reaches its optimum at a solution duration of 3 h, with no significant coarsening observed. At this stage, the fine and rounded Si particles greatly mitigate the splitting effect and stress concentration on the α-Al matrix previously caused by the needle-like structure, establishing the optimal microstructural foundation for the enhancement of the alloy's macro-mechanical properties.

Effect of aging time on microstructure

θ'(Al_2Cu) is the primary precipitation-strengthening phase in ADC12 alloy. Under an aging temperature of 180 °C, the moderate solute precipitation rate facilitates the formation of finely dispersed θ' phases, which effectively exert dislocation pinning effects. For engine blocks with complex geometries, this temperature range ensures robust phase-transformation strengthening while preventing dimensional distortion caused by the abrupt release of residual stresses, thereby achieving a synergistic optimization of mechanical properties and dimensional stability [16].

As illustrated in Figure 8, with the extension of aging time, the morphology and quantity of the lath-like eutectic Si and Fe-rich phases within

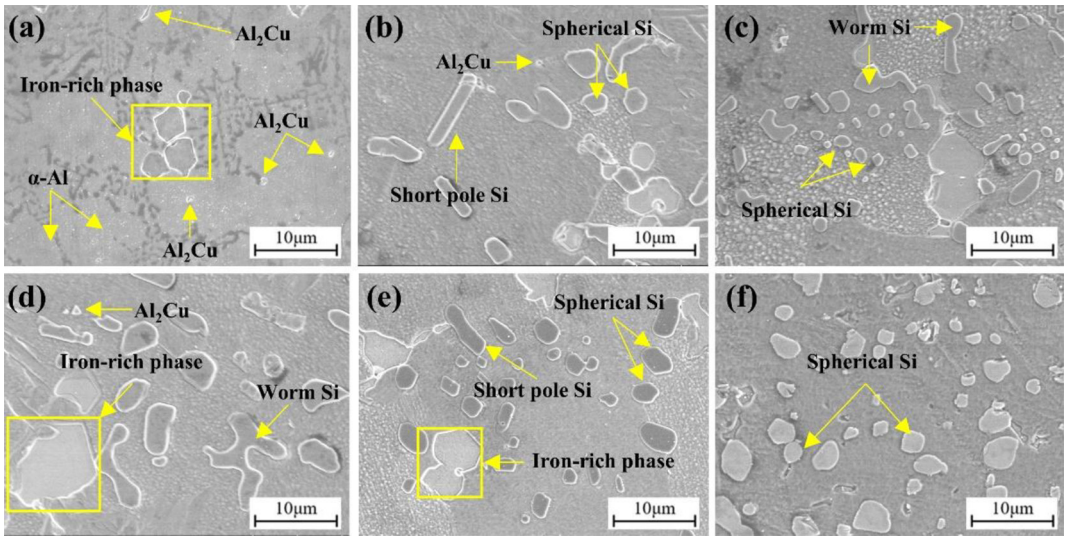

Figure 6. SEM images of ADC12 alloy after solution treatment at 520 °C for different durations: (a) as-cast; (b) 0.5 h; (c) 1 h; (d) 2 h; (e) 3 h; (f) 4 h

the alloy show no significant changes, exhibiting exceptional microstructural stability. During the initial stage of aging, the strengthening particles precipitately dispersed within the alloy possess small diameters that are difficult to observe under an optical microscope, leaving the distribution of eutectic Si and Fe-rich phases relatively distinct. As the aging time extends to 6 h and beyond, a certain number of strengthening particles become visible within the matrix, indicating the continuous precipitation and growth of these phases. With further increases in aging time, the quantity of precipitated strengthening particles increases significantly; they appear uniform in size and are dispersedly distributed without obvious agglomeration. Such uniformly dispersed nanoscale precipitates effectively prevent localized clustering, establishing a structural foundation for the subsequent enhancement of mechanical properties.

The core of the aging process is a thermodynamic sequence: "supersaturated matrix → solute atom diffusion → precipitation of strengthening phases → phase structural stabilization". At an aging temperature of 180 °C, Cu atoms diffuse and aggregate from the supersaturated α-Al matrix, initially forming G.P. zones or transition phases coherent with the matrix. These semi-coherent precipitates induce coherency strain fields in their vicinity, significantly increasing the resistance to dislocation glide and thus endowing the alloy with superior peak strength [17,18]. Due to their high thermal stability, the eutectic Si and Fe-rich phases do not participate in the phase transformations during aging; instead, they serve as a rigid skeleton to maintain the basic morphology of the microstructure, effectively suppressing structural distortion during the aging process.

Effect of aging time on mechanical properties

Figure 9 shows the mechanical properties and elongation of the ADC12 die-cast aluminum alloy under different aging durations. Overall, the tensile strength and yield strength exhibit a highly

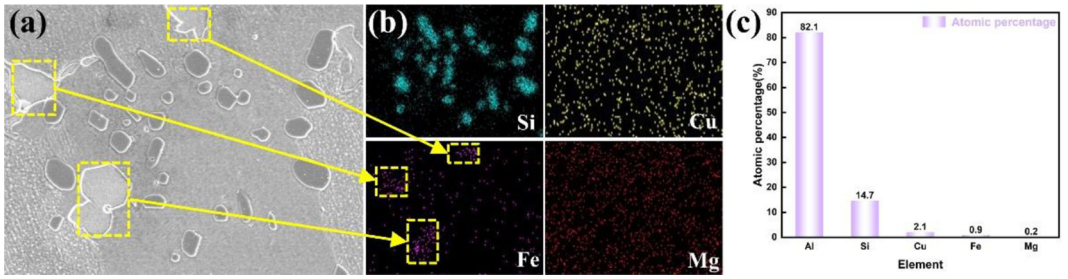

Figure 7. EDS elemental mapping results after solution treatment at 520 °C for 3 h: (a) SEM morphology; (b) elemental distribution; (c) elemental content

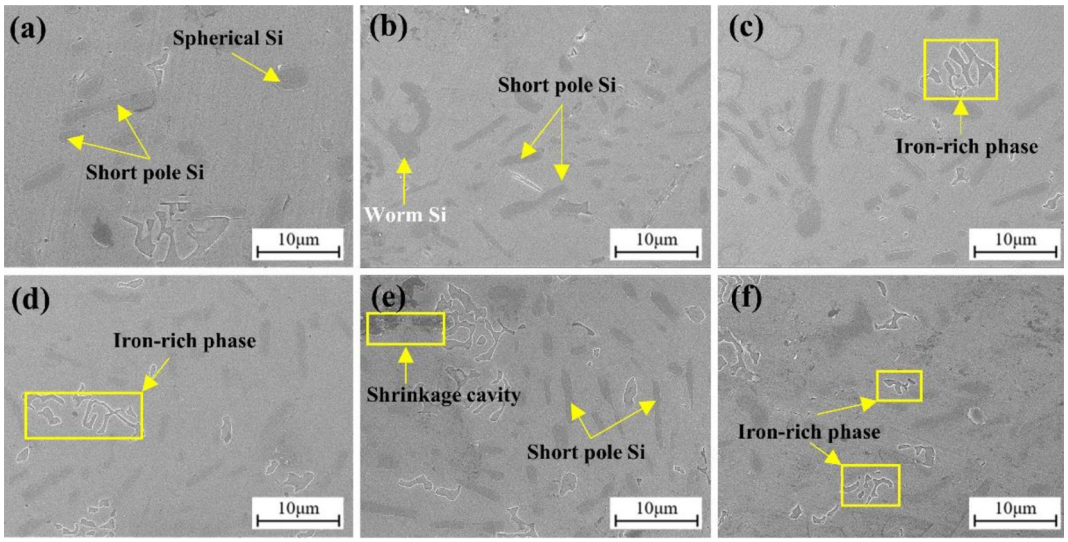

Figure 8. SEM images of ADC12 alloy aging-treated at 180 °C for different durations: (a) 2 h; (b) 4 h; (c) 6 h; (d) 8 h; (e) 10 h; (f) 12 h

consistent "rise–peak–decline" evolution characteristic, while the hardness curve displays a fluctuating trend of a slight initial decrease followed by an increase and a subsequent decline. Notably, a distinct "asynchrony" is observed between the peak times of hardness and strength: the hardness reaches its peak at 8 h of aging, whereas the tensile strength and yield strength do not achieve their maximum levels until 10 h.

Under-aging stage (2–4 h): High residual stresses exist in the solution-treated and quenched matrix, the release of which during early aging leads to a brief, slight decrease in hardness. Subsequently, the segregation of supersaturated Cu atoms drives the preferential nucleation and precipitation of fine G.P. zones and θ'' phases that maintain full coherency with the matrix. At this stage, however, the low volume fraction of these precipitates exerts limited dislocation pinning effects, resulting in relatively low comprehensive mechanical properties. Although the elongation at this stage (2.79–2.97%) is higher than that in the as-cast state, the strength has not yet reached its peak, failing to meet the core load-bearing requirements for engine blocks.

Peak-aging transition zone (6–10 h): At 8 h of aging, highly dispersed θ'' phases coexist with the gradually nucleating fine θ' phases. The θ'' phase maintains a strong coherency with the matrix, inducing a severe localized lattice distortion stress field that maximizes the resistance to localized plastic deformation (indentation) and causes the hardness to peak first. When the aging time extends to 10 h, these metastable phases transform into semi-coherent θ' phases with moderate size and uniform distribution. Although the coherency strain weakens slightly at this stage – leading to a decline in hardness – the volume fraction of the θ' phase reaches its maximum. This optimal matching of microscopic size and volume fraction brings the macro-deformation resistance to its summit, with tensile strength and yield strength peaking at 10 h. At 8 h of aging, the material achieves a tensile strength of 312.8 MPa, a yield strength of 239.6 MPa, and a hardness of 114.5. This effectively resists the cyclic mechanical loads of the engine block and prevents macro-plastic deformation. In terms of ductility, the elongation reaches 3.36%, providing sufficient plastic reserve for fatigue crack inhibition and thermal stress relief.

Over-aging stage (beyond 10 h): Beyond 10 h of aging, the θ' phases undergo coarsening and agglomeration driven by thermodynamics, significantly increasing the inter-particle spacing of the strengthening phases. This microstructural evolution leads to a sharp drop in the critical resolved shear stress required for dislocations to bypass these coarsened particles, manifesting macroscopically as a simultaneous attenuation of both hardness and strength. Nevertheless, as the strengthening phase skeleton remains relatively stable, the mechanical properties at 12 h remain significantly superior to those observed in the initial aging stage. Although the strength slightly regresses, it remains above 318 MPa

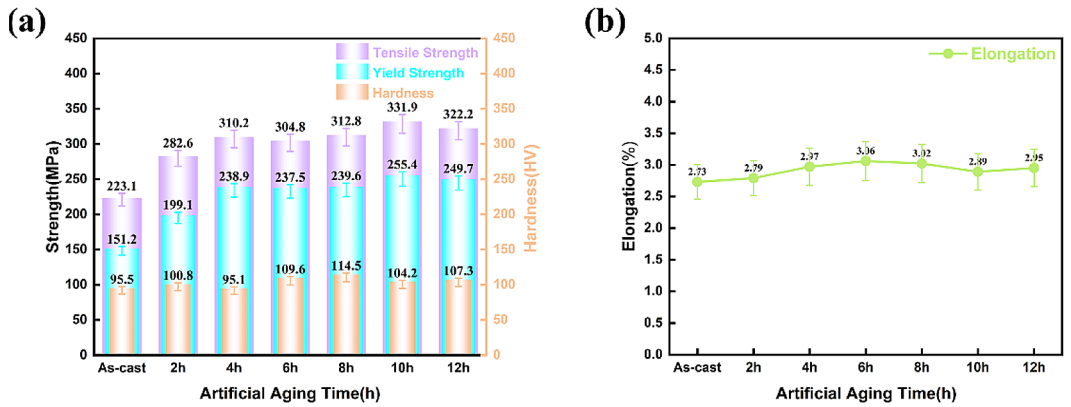

Figure 9. Evolution of mechanical properties during aging treatment at 180 °C: (a) Tensile strength, Yield strength, Hardness; (b) Elongation

– a relatively high level. The elongation drops to 3.19%, which still represents a significant improvement over the as-cast microstructure. From an engineering application perspective, while the material in this state can satisfy the service requirements for light-to-medium duty engine blocks, its fatigue life and thermal shock resistance are inferior to those of the 8-hour aging process, indicating that this is not the optimal processing window.

CONCLUSIONS

In this study, a synergistic strengthening strategy of "die-casting defect control + T6 heat treatment" was proposed to address the casting difficulties and performance bottlenecks of ADC12 aluminum alloy engine blocks. Based on numerical simulations and experimental validation, the following primary conclusions were drawn:

1. Die-casting process optimization: By employing a pouring temperature of 660 °C combined with mold spot cooling devices, the volumes of gas entrainment and shrinkage defects (porosity and cavities) within the engine block were significantly reduced to 3237.06 mm³ and 503.12 mm³, respectively. This process enhanced the matrix density and effectively circumvented the technical risk of surface blistering typically induced during subsequent high-temperature heat treatments.
2. Microstructural evolution and property changes during heat treatment: After solution treatment at 520 °C for 3 h followed by aging at 180 °C, the coarse Al_2Cu phases were fully dissolved into the α-Al matrix, while the Fe-rich phases remained essentially insoluble and segregated at the grain boundaries. The eutectic Si phases underwent complete spheroidization without significant coarsening, effectively mitigating the splitting effect on the matrix. During the aging process, a large number of semi-coherent metastable transition phases precipitated from the matrix. The alloy achieved a peak hardness of 114.5 HV at 8 h of aging, and reached a tensile strength of 331.9 MPa and a yield strength of 255.4 MPa at 10 h, demonstrating a significant precipitation strengthening effect.
3. Process optimization and validation: Considering both mechanical properties and economic efficiency, the 520 °C × 3 h solution treatment + 180 °C × 8 h aging was determined as the optimal T6 treatment process. Following this treatment, the tensile strength and yield strength of the engine block reached 312.8 MPa and 239.6 MPa, respectively – representing significant increases of 40.2% and 58.5% compared to the as-cast state. Additionally, the elongation reached 3.36%. These properties successfully meet the requirements for high-performance service.

Acknowledgements

The authors acknowledge the project of Key Laboratory of Advanced Functional Materials and Devices of Anhui Province (PA2025GDSK0053), Hefei Jianghuai Casting LTD. (W2023JSKF0487) and Anhui Provincial Science and Technology Tackling Key Problems Program (202423i08050007).

REFERENCES

1. Fan Z. Z., Yuan W. Q., Wang D. Z., et al. Research status and future development trend of die casting aluminum alloys. Foundry 2020; 69(02): 159–166.
2. Abboud J., Mazumder J. Developing of nano sized fibrous eutectic silicon in hypereutectic Al–Si alloy by laser remelting. Sci. Rep. 2020; 10(1): 6907. https://doi.org/10.1038/s41598-020-69072-1
3. Dybowski B., Kielbus A., Poloczek L. Effects of die-casting defects on the blister formation in high-pressure die-casting aluminum structural components. Eng. Fail. Anal. 2023; 152: 107223. https://doi.org/10.1016/j.engfailanal.2023.107223
4. Gomes R., Soares G., Madureira R., et al. Development of heat treatments for structural parts in aluminium alloys produced by high-pressure die casting (HPDC). Metals 2024; 14(9): 1059. https://doi.org/10.3390/met14091059
5. Yan H., Chen F. H., Li Z. H. Microstructure and mechanical properties of AlSi10Cu3 alloy with (La+Yb) addition processed by heat treatment. J. Rare Earths 2016; 34(9): 938–944. https://doi.org/10.1016/S1002-0721(16)60118-7
6. Wu Y. F., et al. Effects of pre-aging treatment on subsequent artificial aging characteristics of Al-3.95Cu-(1.32Mg)-0.52Mn-0.11Zr alloys. J. Cent. South Univ. 2015; 22: 2487–2495. https://doi.org/10.1007/s11771-015-2487-9
7. Xiao R., Wang G. J., Meng X. S., et al. Simulation study on integrated bottom car body formation by high pressure die casting with a dual injection system. China Foundry 2025; 22(4): 1–11. https://doi.org/10.1007/S41230-025-4028-Y
8. Cao H., Luo Z., Wang C., et al. The stress concentration mechanism of pores affecting the tensile properties in vacuum die casting metals. Materials 2020; 13(13): 3019. https://doi.org/10.3390/ma13133019
9. Zhang M. Y., Niu X. F., Jia X. L., et al. Parameter optimization of squeezing casting process for aluminum alloy automobile support parts. Spec. Cast. Nonferrous Alloys 2024; 44(10): 1436–1440. https://doi.org/10.15980/j.tzzz.2024.10.025
10. Ren Y. F., Pan X. Y., Wan T. J., et al. Effect of T6 heat treatment on microstructure and properties of high pressure die cast ADC12 aluminum alloy. Heat Treat. Met. 2024; 49(08): 108–112. https://doi.org/10.13251/j.issn.0254-6051.2024.08.017
11. Xu M. W., Zhang X. P., Zhang Q. S., et al. Effect of different aging treatments on the microstructure and corrosion resistance of ADC12 alloy. J. Mater. Eng. Perform. 2023; 33(14): 7074–7086. https://doi.org/10.1007/S11665-023-08486-0
12. Xu Z., Yu L. Z., Li Z. H., et al. Effects of Cu addition on age hardening behavior and mechanical properties of high-strength Al-1.2Mg-1.2Si alloy. Materials 2023; 16(8): 3126. https://doi.org/10.3390/MA16083126
13. Zhang M., Tian Y., Zheng X., et al. Research progress on multi-component alloying and heat treatment of high strength and toughness AlSiCuMg cast aluminum alloys. Materials 2023; 16(3): 1065. https://doi.org/10.3390/ma16031065
14. Yu X., Jiang Z. S., Xu L. J. Microstructure and properties of ADC12 aluminum alloy improved by casting-forging combined forming. Spec. Cast. Nonferrous Alloys 2017; 37(2): 159–162. https://doi.org/10.15980/j.tzzz.2017.02.027
15. Chen W., Liu L., Wei L., et al. Multiphase structure after heat treatment enables a superior strength-plasticity combination in Y-modified ADC12 aluminum alloys. Mater. Tehnol. 2025; 59(4). https://doi.org/10.17222/mit.2024.1296
16. Okayasu M., Go S. Precise analysis of effects of aging on mechanical properties of cast ADC12 aluminum alloy. Mater. Sci. Eng. A 2015; 638: 208–218. https://doi.org/10.1016/j.msea.2015.04.072
17. An H. E., Jie S. L. Effect of heat treatment process on microstructure and properties of ADC12 Al alloy for automobile engine. Hot Work. Technol. 2017; 46(14): 208–211.
18. Canyook R., Utakrut R., Wongnichakorn C., et al. The effects of heat treatment on microstructure and mechanical properties of rheocasting ADC12 aluminum alloy. Mater. Today: Proc. 2018; 5(3): 9476–9482. https://doi.org/10.1016/j.matpr.2017.10.127